Review

Not peer-reviewed version

# Advances in Deep Brain Imaging with Quantum Dots: Structural, Functional, and Disease Specific Roles

Tenesha Connor , Hemal Weerasinghe , Justin Lathia , Clemens Burda , Murat Yildirim *

Posted Date: 13 November 2024

doi: 10.20944/preprints202411.0856.v1

Keywords: quantum dots; multiphoton microscopy; neurological disorders

 doi:10.20944/preprints202411.0856.v1



*Review*

# Advances in Deep Brain Imaging with Quantum Dots: Structural, Functional, and Disease Specific Roles

**Tenesha Connor [1,2], Hemal Weerasinghe [3], Justin Lathia [4-6] Clemens Burda [3] and Murat Yildirim [1]**

[1] Department of Neurosciences, Cleveland Clinic Lerner Research Institute, Cleveland, OH, United States
[2] Department of Chemical and Biomedical Engineering, Cleveland State University, Cleveland, OH, United States
[3] Department of Chemistry, Case Western Reserve University, Cleveland, OH, United States
[4] Department of Cardiovascular and Metabolic Sciences, Cleveland Clinic Lerner Research Institute, Cleveland, OH, United States
[5] Case Comprehensive Cancer Center, Cleveland OH, United States
[6] Rose Ella Burkhardt Brain Tumor and Neuro-Oncology Center, Cleveland Clinic, Cleveland, OH, United States
* Correspondence: yildirm2@ccf.org

**Abstract:** Quantum dots (QDs) have emerged as promising tools in advancing multiphoton microscopy (MPM) for deep brain imaging, addressing long-standing challenges in resolution, penetration depth, and light-tissue interactions. MPM, which relies on nonlinear photon absorption, enables fluorescence imaging within defined volumes, effectively reducing background noise and photobleaching. However, achieving greater depths remains limited by light scattering and absorption, compounded by the need for balanced laser power to avoid tissue damage. QDs, nanoscale semiconductor particles with unique optical properties, offer substantial advantages over traditional fluorophores, including high quantum yields, large absorption cross-sections, superior photostability, and tunable emission spectra. These properties enhance signal to background ratio at increased depths and reduce scattering effects, making QDs ideal for imaging subcortical regions like the hippocampus without extensive microscope modifications. Studies have demonstrated the capability of QDs to achieve imaging depths up to 2100 μm, far exceeding that of conventional fluorophores. Beyond structural imaging, QDs facilitate functional imaging applications, such as high-resolution tracking of hemodynamic responses and neural activity, supporting investigations of neuronal dynamics and blood flow in vivo. Their stability enables long-term, targeted drug delivery and photodynamic therapy, presenting potential therapeutic applications in treating brain tumors, Alzheimer's disease, and traumatic brain injury. This review highlights the impact of QDs on MPM, their effectiveness in overcoming light attenuation in deep tissue, and their expanding role in diagnosing and treating neurological disorders, positioning them as transformative agents for both brain imaging and intervention.

**Keywords:** quantum dots; multiphoton microscopy; neurological disorders

## 1. Introduction

Achieving deep brain imaging has long been constrained by challenges in resolution, penetration depth, and the complex interaction of light with inhomogeneous biological tissues. Multiphoton microscopy (MPM) offers a solution by confining fluorescence to a focused volume through nonlinear photon absorption, which reduces background noise and photobleaching [1]. Yet, factors such as light scattering [2], tissue absorption [3], and the delicate balance of laser power required all impact outcomes of MPM [1]. To address these challenges, it is important to understand the physical principles influencing nonlinear imaging.

In MPM, fluorescence is achieved by multiphoton excitation, when multiple low-energy photons are simultaneously absorbed, causing the fluorophore to fluoresce [4]. For a *n*-photon excitation

 doi:10.20944/preprints202411.0856.v1



process, the fluorescence intensity, $I_f$, depends on both the absorption cross-section and excitation intensity as defined by:

$$I_f \propto \sigma_n \cdot I^n \quad \textbf{(Eq. 1)}$$

where $\sigma_n$ is the absorption cross-section, $I$ is the photon density at the focal point, and $n$ is the number of photons absorbed simultaneously. Here, $\sigma_n$ is critical as a higher absorption-cross section increases simultaneous photon absorption, generating a stronger signal even at reduced laser intensities. This is beneficial for deeper tissue imaging because photon density diminishes with depth due to scattering and absorption [5]. Therefore, attenuation of ballistic photons becomes a major limitation in achieving deeper imaging as explained by Beer-Lambert's law: [6, 7]

$$I(z) = I_0 \cdot e^{(-\mu_t z)} \quad \textbf{(Eq. 2)}$$

where $I_0$ is the initial intensity at the brain surface, $\mu_t = \mu_s + \mu_a$ is the total attenuation coefficient (comprising scattering $\mu_s$ and absorption $\mu_a$ coefficients) [8], and $z$ is imaging depth. In brain tissue, scattering dominates over absorption, particularly in the near-infrared (NIR) window, which is optimal for minimizing light loss [9]. More specifically, scattering is predictably dominant in the range of 700 - 1000 nm and becomes more discrete in the 1000 - 1700 nm range. The exponential decay of ballistic photons can be expressed by:

$$P(z) = P_0 \cdot e^{\left(-\frac{z}{EAL}\right)} \quad \textbf{(Eq. 3)}$$

where $P_0$ is the power at the brain surface and $EAL$ is the effective attenuation length [10]. The exponential decay explains the rapid decrease in laser power with increasing imaging depth. While using longer excitation wavelengths in 3PM (e.g., 1300 nm and 1700 nm) can extend the effective attenuation length (EAL), fluorescence still diminishes with depth due to attenuation effects [3, 11-16]. Additionally, many standard fluorophores have lower absorption cross-sections and quantum yields [17]. As a result, overcoming these combinations of challenges often requires higher laser powers to produce adequate fluorescence signals at greater depths. Yet there still must be a balance in pulse energy, repetition rate, and overall power at the brain surface to ensure damage-free deep brain imaging.

Previous studies have sought to enhance deep tissue imaging by engineering microscope systems or incorporating complex components like adaptive optics (AO). AO plays a critical role by correcting aberrations caused by the tissue's heterogenous refractive index and scattering variations [12]. These aberrations distort the excitation wavefront, enlarging the point spread function (PSF) and reducing both resolution and fluorescence signal [18]. Both direct and indirect AO wavefront sensing methods improve resolution and signal strength at depth [19-21]. For example, 3PFM with AO achieved near diffraction limited performance and a fourfold resolution improvement at 1450 μm depth [22], while 2PFM with direct imaging AO reached depths of 700 μm in mouse brain tissue [23]. Even so, achieving these improvements often requires substantial system modifications, precise calibrations, and specialized expertise. Despite these efforts, the improvements gained is often still limited, making such extensive hardware modifications not only challenging, but also costly.

Achieving deeper imaging depths can be accomplished not only by modifying various aspects of the microscopy setup, but also by utilizing brighter probes. Quantum dots (QDs) have emerged as highly effective probes for this purpose, offering significant advantages over traditional fluorophores [5, 24-27]. QDs are semiconducting nanoscale particles whose distinct optical properties stem from quantum confinement effects, which are directly influenced by their physical size and material composition [28, 29]. A major benefit of QDs is their tunable absorption and emission spectra allowing for custom design to meet specific experimental needs [30]. Their tunable Stokes shifts, creating a clear separation between excitation and emission wavelengths, minimizes overlap, thereby enhancing the SBR, reducing scattering, and enabling more efficient multicolor imaging [30-32].

QDs also exhibit high quantum yields in both the UV-visible range as well as the NIR. Resch-Grenger et al., (2008) reported QD quantum yields as high as 0.65-0.85 in the visible range, exceeding most organic dyes, which typically exhibit quantum yields of 0.3-0.5 in the visible range and even lower values in the NIR range. Additionally, QDs have larger molar absorption coefficients **(Figure 1A, 1B; Table 1)**, extended fluorescence lifetimes **(Figure 1C)** [33, 34], superior photostability [35] and

 doi:10.20944/preprints202411.0856.v1



exceptional brightness compared to other imaging probes [32, 36]. These properties make QDs particularly well-suited for long-term, *in vivo* imaging of deep brain regions, such as the hippocampus or subcortical brain regions [24, 26, 37]. Thus, by utilizing QDs, researchers can achieve unprecedented depths without the need for extensive modifications to the microscopy system.

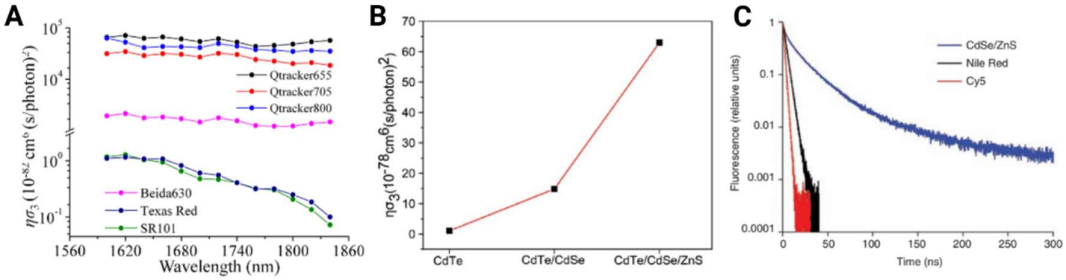


**Figure 1.** Optical properties of various fluorophores used in deep brain imaging **(A)** Comparison of absorption cross section ($\eta\sigma_3$) for commercial QDs (Qtracker) and traditional dyes (Texas Red and SR101) across wavelength 1600 to 1840 nm. Adapted from [25]. **(B)** $\eta\sigma_3$ for lab-created CdTe QDs, showing increased values with additional shell layers (CdSe, CdSe/ZnS) under 1600 nm excitation. Adapted from [36]. **(C)** Fluorescence decay comparison between common fluorophores and CdSe/ZnS QDs. Cy5 and Nile Red exhibit mono-exponential decays with lifetimes of 1.5 ns and 3.6 ns, respectively, while QD displays multi-exponential decay with mean lifetime of 10.3ns, demonstrating significantly longer fluorescence duration. Adapted from [34].

## 2. Advances in Structural Brain Imaging Using Quantum Dots

QDs have propelled advancements in MPM, demonstrating effective use in structural imaging through 2PFM [33, 38], 3PFM [5, 24-27, 39], and 4PFM [24] modalities for *in vivo* visualization of mouse brain vasculature (**Figure 2**). These applications leverage the QDs' superior brightness, larger absorption cross-sections, and use of longer excitation wavelengths (e.g., 1700 nm to 2200 nm) [40-42], which minimizes scattering and optimizes signal retention [1, 2, 43], allowing for deeper imaging while maintaining high SBR ratios [40, 41].

2PM is a widely used bioimaging tool, but its application in the NIR-II range has been limited due to the lack of suitable probes. Nonetheless, recent advances particularly in QDs with modified core and shell properties have made progress in this field possible. For instance, PbS/CdS QDs, emitting fluorescence centered at 1270 nm when excited with a 1550 nm fs laser, allowed for deep brain imaging in the NIR-II range [33]. To further enhance signal detection and resolution, the study combined MPM with fluorescence lifetime imaging to perform two-photon lifetime imaging microscopy (2PFLIM), achieving good contrast at an imaging depth of 220 μm. This marked the first use of 2PFLIM in the NIR-II range for deep-tissue imaging [33]. In a separate study, the integration of an optical parametric oscillator (OPO) in 2PFM demonstrated commercial QDs, like Qtracker655, could achieve imaging depths of approximately 630 μm, compared to 560 μm using NLO alone, (**Figure 2A**) [38].

QDs have also shown considerable potential in 3PFM, offering deep imaging capabilities superior to traditional fluorophores. For instance, excited at 1700 nm, a commercial QD (Qtracker655) enabled imaging depths up to 2100 μm in the mouse brain (**Figure 2B**) [25], far surpassing depths reached by Texas Red dextran (1340 μm) [44] (**Table 1**).

 doi:10.20944/preprints202411.0856.v1



**Table 1.** Multiphoton Imaging Properties of Quantum Dots, Nanoparticles, and Other Fluorophores.

| Material | Preparation | MPM | Absorption Cross-Section | Surgery | Excitation Wavelength Used (nm) | Imaging Depth (μm) | Reference |
|---|---|---|---|---|---|---|---|
| **Fluorescein** | Commercial | 4PF | $\eta\sigma_4$=10.5x10$^{-16}$ cm$^8$ (s/photons)$^3$ | - | 1680 | - | [24] |
| **Qtracker655** | Commercial | 4 PF | $\eta\sigma_4$=7.8x10$^{-108}$ cm$^8$ (s/photons)$^3$ | Intact Skull | 2200 | 330 | [24] |
| | | | | Craniotomy | 2200 | 940 | |
| **Qtracker655** | Commercial | 3PF | $\eta\sigma_3$=7.1x10$^{-78}$ cm$^6$ (s/photons)$^2$ | Craniotomy | 1700 | 2100 | [25] |
| | Commercial | 3PF | - | Intact Skull | 1700 | 750 | [3] |
| **Qtracker800** | Commercial | 3PF | $\eta\sigma_3$=1.68x10$^{-78}$ cm$^6$ (s/photons)$^2$ | Intact Skull | 2200 | 460 | [24] |
| | | | | Craniotomy | 2200 | 1060 | |
| **CdSe/5.8CdS/ZnS QDs** | Lab Modified | 3PF | $\sigma_3$=2.10x10$^{-78}$ cm$^6$ (s/photons)$^2$ | Intact Skull | 1600 | 850 | [26] |
| | | | | Craniotomy | 1600 | 1550 | |
| **CdSe/ZnS QDs** | Lab Modified | 3PF | $\sigma_3$=2.0x10$^{-77}$ cm$^6$ (s/photons)$^2$ | - | 1600 | - | [26] |
| **CdTe QDs** | Lab Modified | 3PF | $\sigma_3$=2.42x10$^{-77}$cm$^6$ (s/photons)$^2$ | - | 1600 | - | [36] |
| | | | $\eta\sigma_3$=1.05x10$^{-78}$ cm$^6$ (s/photons)$^2$ | | | | |
| **CdTe/CdSe QDs** | Lab Modified | 3PF | $\sigma_3$=6.34x10-$^{77}$cm$^6$ (s/photons)$^2$ | - | 1600 | - | [36] |
| | | | $\eta\sigma_3$=14.84x10$^{-78}$cm$^6$ (s/photons)$^2$ | | | | |
| **CdTe/CdSe/ZnS QDs** | Lab Modified | 3PF | $\sigma_3$=25.6x10$^{-77}$cm$^6$ (s/photons)$^2$ | Craniotomy | 1600 | 1300 | [36] |
| | | | $\eta\sigma_3$=62.98x10$^{-78}$cm$^6$ (s/photons)$^2$ | | | | |
| **DCzPDI** | Lab Modified | 3PF | $\sigma_3$=6.8x10$^{-80}$ cm$^6$ (s/photons)$^2$ | Craniotomy | 1550 | 450 | [45] |
| **DCDPP-2TPA** | Lab Modified | 3PF | $\sigma_3$=2.95x10$^{-79}$cm$^6$ (s/photons)$^2$ | Intact Skull | 1550 | 300 | [46] |
| | Lab Modified | | | Craniotomy | 1550 | 785 | |
| **MTTCM NP** | Lab Modified | 3PF | $\eta\sigma_3$=1.13x10$^{-81}$cm$^6$ (s/photons)$^2$ | Intact Skull | 1600 | 1100 | [47] |
| | | | | Craniotomy | 1660 | 1900 | [47] |
| **SR101** | Commercial | 3PF | $\eta\sigma_3$=9.4x10$^{-83}$cm$^6$ (s/photons)$^2$ | - | 1600 | - | [47] |
| **Texas Red dextran** | Commercial | 3PF | - | Craniotomy | 1675 | 1340 | [48] |
| | | 3PF | $\sigma_3$=0.97x10$^{-82}$ cm$^6$ (s/photons)$^2$ | - | 1650 | - | [44] |
| | | 3PF | $\sigma_3$=11x10-82cm6(s/photons)$^2$ | Craniotomy | 1340 | 1200 | [44] |
| | | 3PF | $\eta\sigma_3$=1.2x10$^{-82}$ cm$^6$ (s/photons)$^2$ | - | 1700 | - | [25] |
| | | 3PF | - | Craniotomy | 510 | 510 | [5] |
| **mCherry** | Commercial | 3PF | $\sigma_3$=1.9x10$^{-83}$cm$^6$ (s/photons)$^2$ | - | 1340 | - | [44] |
| **Thy1-EGFP THG imaging** | Transgenic | 3PF | - | Craniotomy | 1300 | 1400 | [22] |
| **mCherry** | Commercial | 2PF | $\sigma_2$=94 cm$^4$ (s/photons) | - | 640-1000 | - | [17] |
| | | 2PF | $\sigma_2$=25 cm$^4$ (s/photons) | - | 1020-1100 | - | |
| **DsRed2** | Commercial | 2PF | $\sigma_2$=104 cm$^4$ (s/photons) | - | 640-1000 | - | |
| | | 2PF | $\sigma_2$=96 cm$^4$ (s/photons) | - | 1020-1100 | - | |
| **PbS/CdS QD** | Lab Modified | 2PF | - | Craniotomy | 1550 | 220 | [33] |
| | | | - | Intact Skull | 1550 | 110 | |
| **CsPbNr3 PQD** | Lab Modified | 2PF | $\sigma_2$=1.8x10$^5$ cm$^4$ (s/photons) | - | 800 | - | [49] |

 doi:10.20944/preprints202411.0856.v1



| | | | | | | | |
|---|---|---|---|---|---|---|---|
| **CsPbI3 QDs** | Lab Modified | 2PF | $\sigma_2$=2.1x10$^6$ cm$^4$ (s/photons) | - | 800 | - | |
| **CsPbCl3 QDs** | Lab Modified | 2PF | $\sigma_2$=3.8x10$^4$ cm$^4$ (s/photons) | - | 800 | - | |
| **Qtracker655** | Commercial | 2PF | - | Craniotomy | 1050 | ~630 | [50] |
| | | | - | | 800 | ~560 | |
| **Texas Red dextran** | Commercial | 2PF | - | Craniotomy | 920 | 420 | [51] |

Figure 2C extends this insight by comparing QDs in 3PFM and 4PFM. In 3PFM, Qtracker800 excited with a 2200 nm wavelength were able to achieve imaging depths of approximately 1060 µm, while 4PFM with Qtracker655 only reached 940 µm [24]. Though theoretically, 4PF could enable deeper penetration due to higher-order nonlinearity, in practice, 3PF achieves greater depths [24]. This is because there is a lower probability of four-photons simultaneously being absorbed with allowable power levels without damaging the brain. In higher photon orders ($n$), the fluorescence signal decays more rapidly due to increased scattering and absorption at depth $z$. Thus, achieving effective signal in 4PF requires elevated pulse energy and power, often nearing or exceeding photodamage thresholds and thereby constraining the theoretical advantage of 4PF imaging.

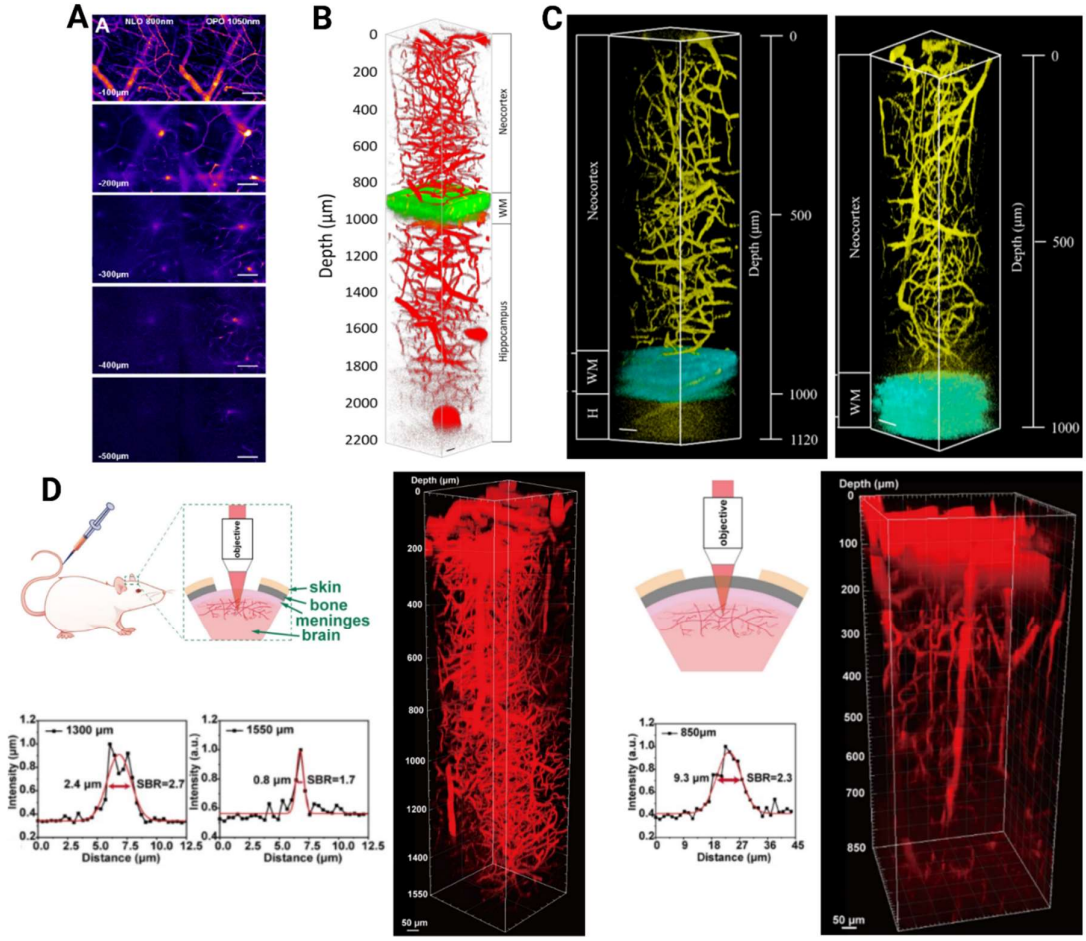


**Figure 2.** Structural multiphoton imaging (*in vivo*) mouse brain vasculature at various depths using quantum dots (QDs) as fluorescent probe. **(A)** Images acquired at depths measured up to ~500 µm below dura-mater utilizing 2P modified microscopy systems comparing 800 nm NLO or 1050 nm OPO excitation in healthy mice intravenously injected with Qtracker655. Adapted from [38] **(B)** 3D reconstruction of 3P imaging of vasculature labeled in red with Qtracker655 illustrating depths deep into the hippocampus (~2100 µm) obtained. Highlighted in green are third-harmonic generation

 doi:10.20944/preprints202411.0856.v1



(THG) signals outlining the white matter (860 -100 μm below surface). Adapted from [25]. **(C)** The yellow color highlights mouse brain blood vessels labeled by QDs excited at 2200 nm. The cyan color shows THG imaging of white matter excited at 1700 nm. Left: 3D reconstruction of 3P imaging of mouse vasculature labeled with Qtracker800 extending to ~1060 μm below surface. Right: 3D reconstruction of 4P imaging of Qtracker655 labeled mouse vasculature extending to ~940 μm below surface. Adapted from [24]. **(D)** 3P imaging of PEGylated CdSe/5.8Cd/ZnS QDs labeled vasculature excited with 1600 nm in healthy mouse brain. Left: Schematic of mouse injected with QDs into the tail before brain imaging a craniotomy. A 3D reconstruction of the blood vessels shows imaging acquired without the skull achieved depths ~1550 μm. Fluorescence intensity and SBR measurements were also obtained at 1300 nm (SBR=2.7) and 1550 nm (SBR=1.7) imaging depths as shown in the two graphs below the schematic. Right: Schematic showing 3P imaging acquired through intact skull. Lower imagining depth is achieved though the skull (~850μm). A 3D reconstruction of the vasculature is presented in the far right. Fluorescence intensity and SBR measurement were obtained at 850 μm (SBR=2.3). Adapted from [26].

Surgical protocols are another factor that must be considered when conducting MPM to image subcortical regions. Craniotomies completely remove the skull to allow laser interactions directly into the brain, therefore, reducing scattering due to the absence of bone [26]. In contrast, imaging through an intact skull introduces additional scattering and absorption obstacles. Figure 2D depicts a schematic of imaging with both a craniotomy (left) and intact skull preparation (right). Bone structure significantly attenuates light, but the strong signal properties of QDs, along with optimized imaging parameters, help to overcome barriers, enabling substantial imaging depth, even under challenging conditions. CdSe/CdS/ZnS QDs were used to label brain vasculature with 3PFM to achieve imaging depths of 1550 μm with craniotomy and 850 μm through an intact skull (**Figure 2D**) [26]. This surpasses imaging depth achieved with commercially available Qtracker800, which only reached 1060 μm with craniotomy and 460 μm through intact skull [24]. Nevertheless, 3PFM vasculature imaging with 1700 nm excited Qtracker655 achieved an imaging depth of 2100 μm with a craniotomy preparation [25] and 750 μm through an intact skull [3]. Achieving such depths, through bone, despite these obstacles is highly promising.

To the best of our knowledge, QDs have not been used in MPM for labeling specific neurons or cell types, *in vivo,* in subcortical regions. Common dyes like fluorescein and rhodamine-derived molecules are typically used to label blood vasculature in the brain [38, 52]. However, their emission spectrum often overlaps with those of other fluorescent proteins, complicating simultaneous imaging of different cell populations. In contrast, Qtracker655, with an emission spectrum centered around 655 nm, enables multicolor imaging by using 1050 nm excitation, allowing simultaneous imaging with Enhanced Yellow Fluorescent Protein (EYFP) or DsRed2 [38]. Ricard et al., (2016) also demonstrated the potential of Qtracker655 for multicolor imaging by successfully labeling neurons with Thy1-CFP, blood vessels with QD655, and dendritic cells/microglia with CD22c-EYFP in a Thy1-CFP/CD11c-EYFP mouse model. Overall, this highlights the utility of QDs for simultaneous visualization of multiple cell types *in vivo* in MPM.

### 3. Exploring Functional Brain Imaging with Quantum Dots

Recent advances in MPM and QD technology have extended beyond structural imaging, to enable high-resolution monitoring of hemodynamic responses [24, 25] and neuronal activity deep within brain tissue [53]. This progress addresses a critical need in neuroscience: the visualization of brain function at cellular resolution in subcortical regions. Through 3PFM, QDs provide unprecedented depth penetration and precise imaging of blood flow dynamics, neural function, and cellular architectures, supporting detailed studies of hemodynamic flow, neuronal activity, and NIR light-stimulated action potentials.

In hemodynamic blood flow studies, QDs allow measurements of flow rates at significant depths within the brain. For example, Qtracker800 enabled *in vivo* 3PFM imaging of blood flow speed at depths 200 μm and 600 μm below the brain surface, recording flow rates of 0.96 mm/s and 0.75 mm/s, respectively [24]. Additionally, Qtracker655-labeled brain vasculature was visualized up to 1600 μm

 doi:10.20944/preprints202411.0856.v1



deep under 1700 nm excitation, far surpassing the capabilities of conventional fluorophores and enabling precise observation of subcortical vascular structures (**Figure 3A**). This visualization of blood flow speeds at such depths demonstrates QDs' robust potential in hemodynamic monitoring [25]. These measurements are important as blood flow dynamics are intricately linked with neural activity and are critical for understanding the physiological basis of various neurological disorders [24].

The brain's intricate architecture and electrochemical network drives complex neural computations and inter-regional communication, fundamental to cognition and behavior. In the past, methods such as *in-vitro* patch-clamping [54, 55], calcium imaging [56], and genetically encoded voltage indicators (GEVIs), [57] have helped decipher neural dynamics. Nevertheless, these approaches are either invasive or limited in temporal resolution, photostability, and response speed. Additionally, these conventional techniques often fall short in capturing rapid neural events due to slower response times and potential photobleaching at higher excitation levels [58, 59]. In comparison, QDs provide high temporal resolution, enabling the detection of single action potential with fewer indicators, critical for tracking fast neural signals without risking toxicity or photodamage [53].

Using a theoretical framework for shot-noise-limited photon detection, simulations quantified the QDs' capability to resolve neural spikes optically. For accurate representation, QDs were sampled at rates exceeding 2 kHz and were able to capture the spike waveform with high fidelity. These simulations further confirmed that QDs' superior brightness enables single spike detection at lower labeling densities than traditional voltage-sensitive dyes (VSDs) or GEVIs (**Figure 3B**). Moreover, QDs are not susceptible to photobleaching and photodamage constraints, unlike conventional fluorophores whose excitation intensities are typically limited to ~1mW/mm$^2$ due to risks of intersystem crossing into long-lived triplet states [60]. Consequently, QDs can sustain high excitation intensities, allowing for efficient spike detection while minimizing the impact on membrane capacitance.

For *in vivo* recordings, QDs have been modified (e.g. QD-JBD1-C60) to detect and respond to electrical stimulation to capture cortical responses in widefield imaging [53]. The fluorescence traces for each region of interest (ROI) show distinct temporal profiles in response to electrical stimulation, with proximal areas displaying a more immediate, robust fluorescence change (**Figure 3C**). This rapid detection reflects QDs' capacity to monitor neural activity with both spatial and temporal precision and usefulness for electrophysiology [53].

Marshall & Schnitzer (2013) explored the potential of QDs as voltage indicators by modeling their excitation and emission dynamics as a two-state system. Here, rate constants for excitation ($k_a$), radiative decay ($k_r$), and nonradiative decay ($k_{nr}$) govern the QD behavior. In semiconductor nanocrystals, photon absorption excites a bound electron-hole pair (exciton) which recombines via radiative or nonradiative processes. The radiative decay rate is given by $k_r = \frac{1}{\tau_r}$, where $\tau_r$, the fluorescence lifetime, is inversely proportional to the overlap between electron and hole wave functions:

$$\tau_r \propto |\langle \psi_e | \psi_h \rangle|^{-2} \qquad \textbf{(Eq. 4)} \quad [59]$$

Focusing on type II-VI semiconductors like CdTe QDs, the difference in effective masses of electrons ($m_e^*$) and holes ($m_h^*$) enhances sensitivity to transmembrane voltages. Effective masses create an energy differential, with energies of the charge carriers inversely proportional to their effective masses. This makes QDs highly sensitive to transmembrane voltages, especially when embedded in or near the cell membrane [59, 61]. Chen et al (2019) synthesized glutathione-capped CdSe/ZnS QDs, emitting at 520 nm, that effectively labeled the plasma membrane of neurons (**Figure 3D**).

Neurons were co-labeled with CdSe/ZnS-GSH QDs (green) and DiD (red) that exhibit clear colocalization, with yellow indicating merged areas, highlighting the QDs' ability to precisely label cell membrane within 30 mins (**Fig 3D**). For CdTe QDs, an electric field strength of approximately 5

 doi:10.20944/preprints202411.0856.v1



mV/nm produces a fluorescence lifetime change of: $\frac{\Delta\tau}{\tau_r} \approx 2.5\%$ [59]. This reinforces QDs' sensitivity to membrane potential shifts and their potential for tracking neuronal activity [53, 59, 61].

Beyond detection, a recent study utilized QDs in bio-interface applications that enable remote neural stimulation **(Figure3E)** [58]. Utilizing NIR light, QD based bio-interfaces stimulated primary neurons by converting light into ionic currents that evoked action potentials without the need for external power sources (**Figure 3E**). This setup allows for deep tissue neuron stimulation without the need for batteries, highlighting potential applications in bioelectronic medicine [58, 62].

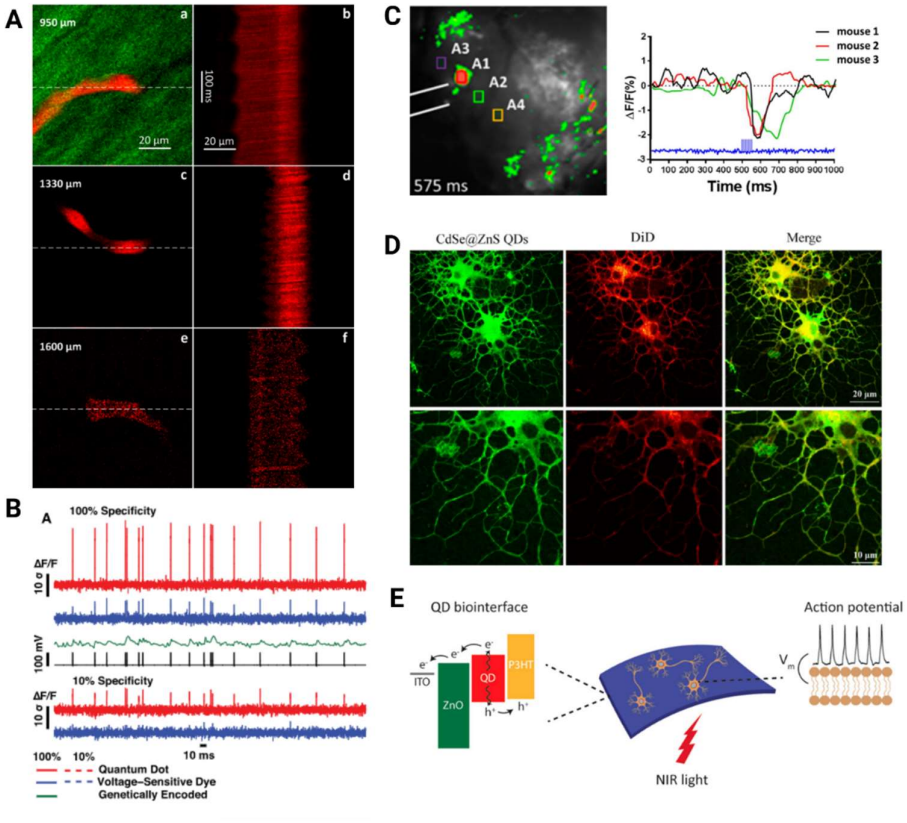


**Figure 3.** QDs in various functional imaging applications in the brain. **(A)** In vivo 3PFM images of Qtracker655-labeled blood vessels at (a) 950 µm, (c) 1330 µm, (e) and 1660 µm below the brain surface. Green signal in (a) shows myelinated axons. Line scans (b,d,f) along dashed lines measure blood flow speed. Pixel:512 x 512. Adapted from [37]. **(B)** Simulated ΔF/F changes for cortical spike trans using QDs, VSDs, and GEVIs, assuming 105 indicators per ell with 100% membrane localization. Sampled at 10 kHz with excitation intensities of 100 mW/mm$^2$. Adapted from [59]. **(C)** In vivo imaging of cortical stimulation with QD-JB1-C60 bioconjugates. (Left) Fluorescence at 575 ms shows four ROIs (A1-A4), with electrode position marked by white lines. (Right) ΔF/F% intensity profiles for ROI A1 across three mice, showing peak response (~2.1%) ~100 ms post-stimulation and return to baseline within 80 -100 ms. Adapted from [53]. **(D)** Fluorescence images of neurons co-labeled with CdSe/ZnS-GSH QDs (green) and DiD (red), with merged images showing colocalization (yellow). DiD, a lipophilic dye embedded in the phospholipid bilayer, highlights cell membranes. The overlap of the images confirm the QDs correctly labeled the cell membranes of neurons. Adapted from [61]. **(E)** Flexible QD biointerfaces for photomodulation of neurons using NIR light. NIR light stimulates neurons in primary hippocampal neurons *in vitro* to generate safe capacitive ionic currents that generate action potentials. Adapted from [58].

 doi:10.20944/preprints202411.0856.v1



**4. Synthesis Mechanisms of Quantum Dots for Enhanced Multiphoton Imaging**

When selecting a QD for experimentation, researchers can opt for commercially available options like Qtracker products or custom lab-synthesized QDs. Commercial QDs offer convenience and consistency, as they are pre-functionalized for general applications and span a range of excitation and emission wavelengths compatible with common imaging systems. Qtracker QDs are specifically designed to be injected into the tail vein of mice to study vascular structures. The core is coated with polyethylene glycol (PEG) to reduce nonspecific binding interactions and allows imaging for up to three hours post-injection [63]. Alternatively, lab-synthesized QDs offer greater flexibility, allowing for customization of optical and functional properties to meet specific experimental needs, and are often a more cost-effective option.

When designing QDs for biomedical imaging, it is important to consider the composition of each component: core, shell, and surface ligands. The core properties, such as size, geometry, and chemical composition play a critical role in optimizing photophysical characteristics. Additionally, QDs must be water-soluble to be effective in biological environments. For the shell, considerations include stability, biocompatibility, and effective anchoring of ligands, as the shell shields the QD core from the biological environment. Surface ligands further enhance biofunctionalization by providing stability, maintaining ligand activity, and allowing controlled attachment of functional groups, which are necessary for biological interactions [64].

The synthesis of NIR QDs typically involves methods like hot-injection, heat-up, microwave, and hydrothermal techniques, each providing specific advantages for optimization [64] (**Figure 4A**). The hot-injection technique enables precise control over particle size and emission peaks by rapidly injecting precursors into a hot coordinating solvent, resulting in uniform cores with high quantum yields and photostability, ideal for stable *in vivo* imaging [5, 27, 65]. Hydrothermal and solvothermal methods, which use high temperatures and pressures in sealed vessels, help to enhance QD crystallinity and control particle size [66]. These methods have been used to make biocompatible, nitrogen-doped carbon QDs that can cross the blood brain barrier (BBB) [67, 68].

Other synthesis approaches, such as heat-up and microwave methods can be combined with traditional techniques. The heat-up method, which does not require a rapid injection step, involves a single pot reaction that provides a slower, more controlled nucleation phase, but necessitates the use of reagents with closely matched reactivity to ensure uniform nucleation [69]. The hydrothermal technique relies on hot pressurized aqueous solvents to produce monodisperse QDs that are compatible with aqueous media, without post-synthesis treatments [66]. This method is frequently applied for biological compatible QDs [70]. Recent studies have combined solvothermal and microwave methods to create NIR-emitting carbon QDs utilized in imaging studies [67].

Bandgap engineering further improves QD performance in 3PF applications. Recent studies have introduced an intermediate layer between a CdSe [26] or CdTe [36] core and a ZnS shell, forming a quasi-type II configuration **(Figure 4B)**. This structure significantly improves the absorption cross-section and boosts three photon fluorescence efficiency. Likewise, the ZnS shell provides electronic passivation, enhanced quantum yield, and makes the QD more robust, all which support prolonged imaging stability [26]. Adding a CdS interlayer minimizes lattice mismatch between the core and shell, effectively reducing non-radiative recombination [26]. Intrinsic polarization effects also makes shell thickness a key factor in determining the absorption cross-section [26, 36]. Consequently, precise engineering of both the composition and structure of the shell is essential for optimizing QD performance.

Furthermore, QDs can be engineered to target specific cell types for both structural and functional imaging as previously described. For example, to visualize cellular membrane potentials, QDs such as the QD-peptide-$C_{60}$ bioconjugate complex have been developed [53] (**Figure 4C**). Precise spatial interactions within the cell membrane are critical to the modular design of these type of QDs. The QDs are comprised of a core/shell scaffold that serves as a stable structure, with peptide chains modified to include $C_{60}$ fullerene units attached at specific positions. These peptides self-assemble onto the QD surface via an N-terminal polyhistidine sequence, allowing for controlled binding to the QD shell. By strategically placing a lysine residue within each peptide sequence, $C_{60}$ fullerenes can be

 doi:10.20944/preprints202411.0856.v1



covalently attached through EDC chemistry, creating varied QD-$C_{60}$ separation distances for optimized spatial positioning. Additionally, the peptide chain contain alanine- and leucine-rich regions that form helical structures, facilitating effecting insertion into the cell membrane [53]. These techniques can be utilized in additional studies to create various QDs able to track cellular membrane electrochemical processing.

In addition, surface modifications, like PEGylation are commonly applied to QDs to maintain stability in circulation and enhance biocompatibility (**Figure 4D**) [34, 71-73]. These processes helps to facilitate QD

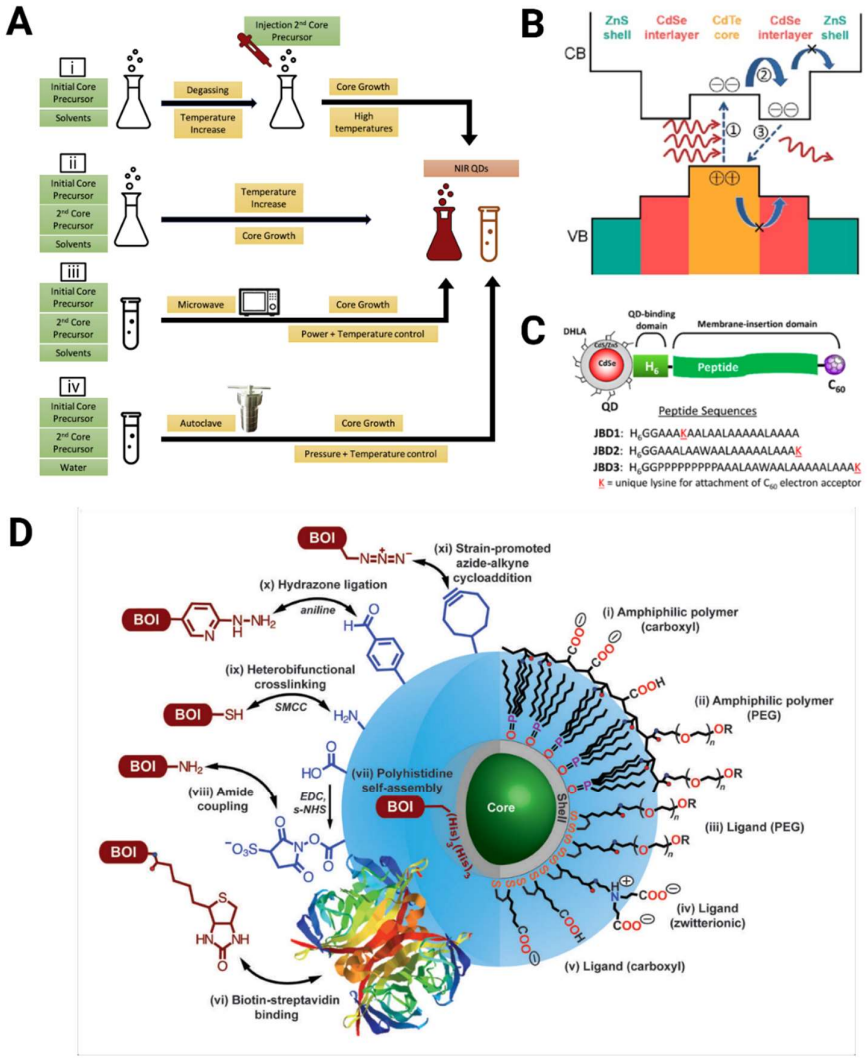


**Figure 4.** Schematic representations of synthesis methods and modifications utilized to create QDs for deep brain imaging and neuron tracking **(A)** Depiction of four NIR QD synthesis methods including, i) Hot Injection: sequential precursor addition at high temperature ii) Heat up: gradual temperature increase after mixing all precursors. iii) Microwave: rapid heating via microwave for core growth. iv) Hydrothermal: high pressure, high temperature growth in an autoclave. Adapted from [64]. **(B)** Depiction of bandgap engineering strategies to create specific band structure alignments in Cd/CdSe/ZnS QDs with a type II configuration, resulting in enhanced 3P fluorescence efficiency. Adapted from [36] **(C)** Representation of a modular design for a targeted approach for QD-based bioconjugates to enhance membrane potential visualization with varying electron acceptor distances. Adapted from [53]. **(D)** Schematic illustration of various bioconjugation techniques (left) biomolecules of interest and (right) surface coating approaches for QDs. Two main coating methods: amphiphilic polymer encapsulation (i,ii) and cap exchange with hydrophilic ligands (iii-v). Adapted from [74].

 doi:10.20944/preprints202411.0856.v1



accumulation in brain tissue, which is particularly useful for long term imaging applications [34]. Targeting ligands, such as asparagine-glycine-arginine (NGR) peptides, can further direct QDs to specific receptors, such as CD13 in gliomas, supporting BBB penetration and targeted tumor imaging. There are two main surface-coating strategies: encapsulation with amphiphilic polymers, which include PEG and carboxylated polymers and cap exchange with hydrophilic ligands such as zwitterionic and carboxylate ligands. Additionally, bioconjugation methods like biotin-streptavidin binding, amide coupling, and strain promoted azide-alkyne cycloaddition (SPAAC) allow for the attachment of biomolecules of interest (BOIs).

## 5. Quantum Dots in the Study, Diagnosis, and Treatment of Neurological Pathologies and Diseases

In recent studies, QDs have demonstrated significant potential in targeting and treating neurological diseases, particularly for conditions such as brain tumors, Alzheimer's disease (AD) and traumatic brain injuries (TBI). The unique properties of QDs discussed thus far, combined with their capability to cross the blood-brain barrier (BBB) make them particularly valuable for both imaging and therapeutic applications **(Figure 5)**.

Gliomas, which represent the most common primary brain tumors, infiltrate healthy brain tissue, and are notoriously challenging to treat. The rapid spread of tumor cells and resistance to conventional treatment leads to high recurrence rates and a median survival rate of less than two years for Grade 4 gliomas, which are commonly referred to as glioblastoma [79, 80]. In vivo imaging has provided key insight into the dynamics of cellular heterogeneity [81, 82] and more recently tumor-neuron interactions [83, 84] and cell invasion [85, 86]. Building on these technological platforms, advanced imaging techniques that clearly delineate tumor boundaries are therefore crucial to improve surgical outcomes [87]. Functionalized QDs, present as a promising tool, particularly PEGylated QDs conjugated with asparagine-glycine-arginine (NGR)-based peptides, which specifically recognize tumor cells. In glioma models, these NGR- functionalized QDs, administered through the rat tail vein, successfully crossed the BBB and selectively accumulated in glioma sites with minimal distribution in healthy brain tissue [75] **(Figure 5B)**. In other models, QD ITK amino (PEG) QDs have co-localized with macrophages in glioma cells without causing significant toxicity to other cells [88]. This has led to accurate glioblastoma detection while supporting the idea that QD can be a safe tool for targeted imaging, therapy, and surgical resection in glioblastoma.

Furthermore, photodynamic therapy (PDT) using QDs is emerging as a promising approach for targeted glioma treatment **(Fig 5A)**. Following injection, functionalized QDs accumulate within tumor cells by selectively binding through ligands that recognize tumor-specific markers [78]. Once localized, these QDs enable precise imaging and mapping of the tumor with MPM, which focuses high-intensity light on subcellular regions within brain tissue. This level of precision has allowed for image-guided laser ablation with precise subcellular targeting of glioblastomas [89]. In addition, specifically engineered QDs can be used to generate reactive oxygen species (ROS) under specific light exposure, causing direct tumor destruction via apoptosis and necrosis. This method can further induce vascular damage within tumors, limit oxygen and nutrient supplies, or stimulate anti-tumor immune responses, all which contribute to effective tumor elimination [90-93]. As research progresses, these guided QD therapies hold promise for treating hard to reach brain tumors with minimal invasiveness and reduced side effects, providing a novel, highly specific approach to target glioma cells deep within the brain [90-93].

QDs have also shown considerable potential in imaging and monitoring traumatic brain injury (TBI), providing valuable insight into injury progression and therapeutic assessment [94]. In mice, NIR-II emitting, silver indium selenide-based and PEG-capped QDs enable real-time tracking of cerebral blood flow and inflammatory responses. These are key elements in understanding TBI pathology.

 doi:10.20944/preprints202411.0856.v1



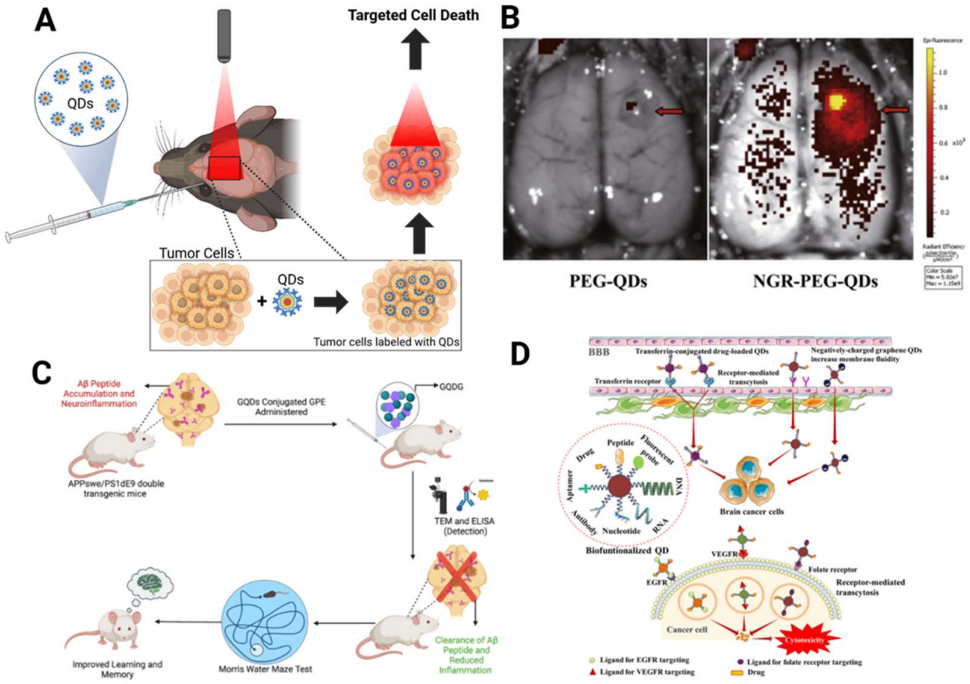


**Figure 5.** Utilizing QDs for neurological applications in pathologies and disease. **(A)** Schematic illustration of the use of QDs for targeting imaging and therapy of brain tumors. QDs selectively accumulate in tumor cells, enabling their specific visualization with MPM, which can then be used therapeutically to induce targeted cell death. Designed using Biorender. **(B)** In vivo glioma imaging in rats 8 hours post-injection with PEG-QDs (left) and NGR-PEG-QDs (right). Fluorescence is negligible with PEG-QDs but pronounced at the tumor site with NGR-PEG-QDs, enhancing glioma detection. Adapted from [75] **(C)** Schematic of GQD-GPE treatment in APP/PS1 mice, targeting Aβ accumulation and neuroinflammation. GQDG administration led to Aβ clearance, reduced inflammation, and improved memory. Adapted from [76, 77]. **(D)** Schematic representation of biofunctionalized QDs delivering drugs across the BBB via receptor-mediated transcytosis, targeting brain cancer cells. Once inside, QDs bind specific receptors (e.g. EGFR, VEGFR, folate) to release drugs and induce cytotoxicity. Adapted from [78].

The engineered QDs facilitated TBI evaluation both pre- and post-surgery. The real time imaging capability provided guidance on the evaluation of intracranial hematomas, supporting critical intraoperative decision-making. QDs further allowed precise monitoring of secondary injuries, offering a 2.5-fold increase in the signal intensity ratio of TBI to normal brain tissue. This enhanced contrast underscores QDs' effectiveness in distinguishing injury-affected areas from healthy brain tissue, aiding in real time assessment of TBI status across different stages of intervention and recovery [94].

Graphene QDs (GQDs) have demonstrated therapeutic effects in Alzheimer's Disease (AD), notably by reducing amyloid-beta (Aβ) accumulation and neuroinflammation [77, 95]. QDs conjugated with neuroprotective peptide glycine-proline-glutamate (GQDG) were administered to an AD transgenic mouse model (APP/PS1). The treatment led to a reduction in inflammatory cytokines and an increase in anti-inflammatory cytokines compared to controls. Other notable changes include increased dendritic spine numbers and improvements in learning and memory as demonstrated by an enhanced performance in the Morris Water Maze, a test where AD models typically perform poorly (**Figure 5C**) [77]. Complementing these results, another study demonstrated GQDs could prevent Aβ aggregation by forming electrostatically driven aggregates with Aβ peptides. These aggregates, ranging from 100-900 nm, generated a cross-linked network structure that was highly unstable and eventually collapsed, effectively inhibiting the Aβ accumulation [95].

 doi:10.20944/preprints202411.0856.v1



This dual effect of GQDs, disrupting Aβ aggregation and reducing neuroinflammation, positions QDs as noteworthy treatment for addressing both the pathological and cognitive deficits of AD.

An alternative therapeutic approach by QDs is their use in cell-specific drug delivery. Biofunctionalized QDs can facilitate receptor-mediated transcytosis, enabling precise drug targeting across the BBB **(Figure 5D)** [78]. QDs can be functionalized with ligands like EGFR, VEGFR, and folate receptors to precisely target brain cancer cells and deliver cytotoxic agents directly to tumor sites [78, 96]. After administration, QDs accumulate in targeted tissue either through receptor-mediated endocytosis or by light-induced ionic interaction that open ion channels. Various conjugated ligands such as peptides, antibodies, nucleic acids, and aptamers, enhance QD specificity for brain tumor cells, improving delivery precision and reducing off-target effects [97-99]. Once inside the cell, QDs can undergo lysosomal degradation, releasing drugs directly into the cytosol, with the QD's biocompatibility and surface modifications directly influencing their biological half-life and metabolism [100].

## 6. Conclusions

QDs have tremendous potential in the field of neuroscience and optical imaging, offering unprecedented capabilities in both deep brain imaging and targeted treatment of neurological disorders. Their unique optical properties, including high brightness, stability, tunable excitation and emission spectra, and customizable functionalities enable applications that significantly exceed those of conventional fluorophores. Notably, QDs have shown utility in precise monitoring of cellular dynamics, hemodynamic responses, and neuronal activity at previously inaccessible depths.

In structural imaging, QDs have proven invaluable in MPM due to their large absorption cross-sections and effectiveness in the NIR range, thereby reducing scattering and enabling visualization of subcortical regions like the hippocampus. QD-based imaging has achieved depths up to 2100 μm, demonstrating a powerful approach for studying brain architecture and activity *in vivo*. Combining QDs with other advancement techniques such as adaptive optics could provide real time correction of tissue induced aberrations and further enhance both imaging depth and resolution. Future research might focus on developing QDs with even better optical properties and target imaging of neurons, glial cells, as well as cerebral vessels.

QDs have also been shown to provide a robust platform for capturing rapid neural events and monitoring hemodynamic flow with high temporal resolution. Their stability and compatibility with long-term imaging further enhance their utility in therapeutic applications, including targeted drug delivery, photodynamic therapy, and image guided surgery. Therefore, QDs hold promise in bridging the divide between diagnostic imaging and therapeutic intervention. In the future, QDs could enable simultaneous imaging and treatment, allowing researchers to track therapeutic responses with cellular precision and to refine interventions in real time. Integrating QD-based imaging with targeted treatment for conditions like gliomas, TBI, and AD could pave the way for personalized, image-guided therapies. With ongoing advances in QD synthesis, targeted specificity, and biocompatibility, QDs are poised to become an essential tool, offering an innovative platform for exploring and treating neurological disorders with unparalleled depth, precision, and therapeutic efficiency.

## References

1. Xu, C., et al., *Multiphoton fluorescence excitation: new spectral windows for biological nonlinear microscopy.* Proc Natl Acad Sci U S A, 1996. **93**(20): p. 10763-8.
2. Vellekoop, I.M. and A.P. Mosk, *Focusing coherent light through opaque strongly scattering media.* Opt Lett, 2007. **32**(16): p. 2309-11.
3. Horton, N.G., et al., *In vivo three-photon microscopy of subcortical structures within an intact mouse brain.* Nat Photonics, 2013. **7**(3): p. 205-9.
4. Boyd, R., *Nonlienar Optics.* Academic Press, 2008. **3**.
5. Wang, T., et al., *Three-photon imaging of mouse brain structure and function through the intact skull.* Nat Methods, 2018. **15**(10): p. 789-792.

 doi:10.20944/preprints202411.0856.v1




6. Beer, A., *Bestimmung der Absorption des rothen Lichts in farbigen Flussigkeiten.* Annual Physics, 1852. **162**: p. 78-88.
7. Lambert, J.H., *Photometria siva de mensura et gradibus luminis, coloum et umbrae.* 1760.
8. Izatt, J.A., et al., *Optical coherence microscopy in scattering media.* Opt Lett, 1994. **19**(8): p. 590-2.
9. Shi, L., et al., *Transmission in near-infrared optical windows for deep brain imaging.* J Biophotonics, 2016. **9**(1-2): p. 38-43.
10. Akbari, N., et al., *Imaging deeper than the transport mean free path with multiphoton microscopy.* Biomed Opt Express, 2022. **13**(1): p. 452-463.
11. W. Denk, J.S., and W. Webb, *Two photon laser scannign fluorescence microscopy.* Science, 1990. **248**: p. 73-76.
12. P. Theer, W.D., *On the Fundamental Imaging-depth Limit in Two Photon Microscopy.* Journal of Optical Society, 2006. **23**: p. 3139-49.
13. Xiao, Y., et al., *Three-photon excited fluorescence imaging in neuroscience: From principles to applications.* Front Neurosci, 2023. **17**: p. 1085682.
14. Yildirim, M., et al., *Functional imaging of visual cortical layers and subplate in awake mice with optimized three-photon microscopy.* Nat Commun, 2019. **10**(1): p. 177.
15. Yildirim, M., et al., *Label-free three-photon imaging of intact human cerebral organoids for tracking early events in brain development and deficits in Rett syndrome.* Elife, 2022. **11**.
16. Yildirim, M., et al., *Quantitative third-harmonic generation imaging of mouse visual cortex areas reveals correlations between functional maps and structural substrates.* Biomed Opt Express, 2020. **11**(10): p. 5650-5673.
17. Drobizhev, M., et al., *Absolute two-photon absorption spectra and two-photon brightness of orange and red fluorescent proteins.* J Phys Chem B, 2009. **113**(4): p. 855-9.
18. Turcotte, R., Y. Liang, and N. Ji, *Adaptive optical versus spherical aberration corrections for in vivo brain imaging.* Biomed Opt Express, 2017. **8**(8): p. 3891-3902.
19. Ji, N., *Adaptive optical fluorescence microscopy.* Nat Methods, 2017. **14**(4): p. 374-380.
20. Sinefeld, D., et al., *Three-Photon Adaptive Optics for Mouse Brain Imaging.* Front Neurosci, 2022. **16**: p. 880859.
21. Sinefeld, D., et al., *Adaptive optics in multiphoton microscopy: comparison of two, three and four photon fluorescence.* Opt Express, 2015. **23**(24): p. 31472-83.
22. Streich, L., et al., *High-resolution structural and functional deep brain imaging using adaptive optics three-photon microscopy.* Nat Methods, 2021. **18**(10): p. 1253-1258.
23. Wang, K., et al., *Direct wavefront sensing for high-resolution in vivo imaging in scattering tissue.* Nat Commun, 2015. **6**: p. 7276.
24. Tong, S., et al., *In Vivo Deep-Brain 3- and 4-Photon Fluorescence Imaging of Subcortical Structures Labeled by Quantum Dots Excited at the 2200 nm Window.* ACS Nano, 2023. **17**(4): p. 3686-3695.
25. Liu, H., et al., *In Vivo Deep-Brain Structural and Hemodynamic Multiphoton Microscopy Enabled by Quantum Dots.* Nano Lett, 2019. **19**(8): p. 5260-5265.
26. Wang, F., et al., *Band Gap Engineering Improves Three-Photon Luminescence of Quantum Dots for Deep Brain Imaging.* Anal Chem, 2023. **95**(29): p. 10947-10956.
27. Yang, P., S. Wang, and N. Murase, *Near-infrared emitting CdTe0.5Se0.5/Cd0.5Zn0.5S quantum dots: synthesis and bright luminescence.* Nanoscale Res Lett, 2012. **7**(1): p. 615.
28. Kang, K.I., et al., *Confinement-enhanced biexciton binding energy in semiconductor quantum dots.* Phys Rev B Condens Matter, 1993. **48**(20): p. 15449-15452.
29. Reed, M.A., et al., *Observation of discrete electronic states in a zero-dimensional semiconductor nanostructure.* Phys Rev Lett, 1988. **60**(6): p. 535-537.
30. Yu, G.T., et al., *Molecular Targeting Nanoprobes with Non-Overlap Emission in the Second Near-Infrared Window for in Vivo Two-Color Colocalization of Immune Cells.* ACS Nano, 2019. **13**(11): p. 12830-12839.
31. Park, J., et al., *CuInSe/ZnS core/shell NIR quantum dots for biomedical imaging.* Small, 2011. **7**(22): p. 3148-52.
32. Zhao, P., et al., *Near infrared quantum dots in biomedical applications: current status and future perspective.* Wiley Interdiscip Rev Nanomed Nanobiotechnol, 2018. **10**(3): p. e1483.
33. Huwei Ni, Y.W., Tao Tang, Wenbin Yu, Dongyu Li, Mubin He, Runze Chen, Mingxi Zhang, and Jun Qian, *Quantum Dots Assisted In Vivo Two-Photon Microscopy with NIR-II Emission.* Photonics Research, 2021. **10**(1).
34. Resch-Genger, U., et al., *Quantum dots versus organic dyes as fluorescent labels.* Nat Methods, 2008. **5**(9): p. 763-75.
35. Zhao, S.M., et al., *Aberration corrections for free-space optical communications in atmosphere turbulence using orbital angular momentum states.* Opt Express, 2012. **20**(1): p. 452-61.
36. Yang, J., et al., *Improving Three-Photon Fluorescence of Near-Infrared Quantum Dots for Deep Brain Imaging by Suppressing Biexciton Decay.* Nano Lett, 2024. **24**(22): p. 6706-6713.
37. H Liu, X.D., Shen Tong, Chen He, Hui Cheng, Ziwei Zhuang, Mengyao Gan, Jia Li, Weixin Xie, Ping Qiu, Ke Wang, *In vivo deep brain structural and hemodynamic multiphoton miroscopy enabled by quantum dots.* Nano Letters, 2019. **19**.
38. Ricard, C., et al., *Combination of an optical parametric oscillator and quantum-dots 655 to improve imaging depth of vasculature by intravital multicolor two-photon microscopy.* Biomed Opt Express, 2016. **7**(6): p. 2362-72.

 doi:10.20944/preprints202411.0856.v1




39. Wang, Y., et al., *Aggregation-Induced Emission Luminogen with Deep-Red Emission for Through-Skull Three-Photon Fluorescence Imaging of Mouse.* ACS Nano, 2017. **11**(10): p. 10452-10461.
40. Shen Tong, J.Z., X Chen, X Deng, J Huang, Y Zhang, M Qin, Z Li, Hui Cheng, W Zhang, Lei Zheng, Weixin Xie, Ping Qui, Ke Wang, *In vivo deep brain 3 and 4 photon fluorescence imaging of subbcortical structures labeled by quantum dots excited at the 2200 nm window.* ACS Nano, 2023. **17**: p. 3686-3695.
41. Zhong, J., et al., *In vivo deep brain multiphoton fluorescence imaging emitting at NIR-I and NIR-II and excited at NIR-IV.* J Biophotonics, 2024. **17**(4): p. e202300422.
42. Dan Li, X.D., Zhourui Xu, Deliang Wang, Gaixia Xu, Pingyu Zhang, Ping Qiu, Weixin Xie, Dong Wang, Ben Zhong Tang, Ke Wang, *Molecular Engineering of NIR-II AIE Luminogen Excited at 1700 nm for Ultradeep Intravital Brain Two-Photon Fluorescence Imaging*. Advanced Funtional Materials, 2023. **33**.
43. Webb, C.X.a.W., *Multiphoton Excitation of Molecular Fluorophores and Nonlinear Laser Microscopy*, in *Topics in Fluorescence Spectroscopy*, J.L.P. Press, Editor. 1997. p. 471-540.
44. Yusaku Hontani, F.X., Chris Xu, *Multicolor Three-Photon Fluorescence Imaging with Single-Wavelength Excitation Deep in Mouse Brain.* Science Advances, 2021. **7**.
45. Zhang, K., et al., *Second Near-Infrared (NIR-II) Window for Imaging-Navigated Modulation of Brain Structure and Function.* Small, 2023. **19**(14): p. e2206044.
46. Tang, T., et al., *Nanoprobe-mediated precise imaging and therapy of glioma.* Nanoscale Horiz, 2021. **6**(8): p. 634-650.
47. Deng, X., Xu, Z., Zhang, Z., Zhang, W., Li, J., Zheng, L., Chen, X., Pan, Y., Qui, P., Wang, D., Xu, G., Wang,K, *In Vivo 3-Photon Fluorescence Imaging of Mouse Subcortical Vasculature Labeled by AIEgen Before and After Craniotomy.* Advanced Functional Materials, 2022. **32**(43).
48. Hontani, Y., et al., *Deep-Tissue Three-Photon Fluorescence Microscopy in Intact Mouse and Zebrafish Brain.* J Vis Exp, 2022(179).
49. Pramanik, A., et al., *Water-Soluble and Bright Luminescent Cesium-Lead-Bromide Perovskite Quantum Dot-Polymer Composites for Tumor-Derived Exosome Imaging.* ACS Appl Bio Mater, 2019. **2**(12): p. 5872-5879.
50. Clement Richard, L.L., Alexandre Jaouen, Genevieve Rougon, and Frank Debarbieux, *Combination of an Optical Parametric Oscillator and Quantum-Dots 655 to Improve Imaging Depth of Vasculature by Intravital Multicolor Two-Photon Microscopy.* Biomedical Optics Express, 2016. **7**(6).
51. Fan, J.L., et al., *High-speed volumetric two-photon fluorescence imaging of neurovascular dynamics.* Nat Commun, 2020. **11**(1): p. 6020.
52. Verant, P., et al., *Subtraction method for intravital two-photon microscopy: intraparenchymal imaging and quantification of extravasation in mouse brain cortex.* J Biomed Opt, 2008. **13**(1): p. 011002.
53. Nag, O.K., et al., *Quantum Dot-Peptide-Fullerene Bioconjugates for Visualization of in Vitro and in Vivo Cellular Membrane Potential.* ACS Nano, 2017. **11**(6): p. 5598-5613.
54. Sakmann, B., et al., *Patch clamp techniques used for studying synaptic transmission in slices of mammalian brain.* Q J Exp Physiol, 1989. **74**(7): p. 1107-18.
55. Sakmann, B. and E. Neher, *Patch clamp techniques for studying ionic channels in excitable membranes.* Annu Rev Physiol, 1984. **46**: p. 455-72.
56. Broussard, G.J., R. Liang, and L. Tian, *Monitoring activity in neural circuits with genetically encoded indicators.* Front Mol Neurosci, 2014. **7**: p. 97.
57. Tsytsarev, V., et al., *Recent progress in voltage-sensitive dye imaging for neuroscience.* J Nanosci Nanotechnol, 2014. **14**(7): p. 4733-44.
58. Karatum, O., et al., *Electrical Stimulation of Neurons with Quantum Dots via Near-Infrared Light.* ACS Nano, 2022. **16**(5): p. 8233-8243.
59. Marshall, J.D. and M.J. Schnitzer, *Optical strategies for sensing neuronal voltage using quantum dots and other semiconductor nanocrystals.* ACS Nano, 2013. **7**(5): p. 4601-9.
60. Dombeck, D.A., et al., *Imaging large-scale neural activity with cellular resolution in awake, mobile mice.* Neuron, 2007. **56**(1): p. 43-57.
61. Chen, G., Zhang, Y., Peng, Z., Huang, D., Li, C., Wang, Q., *Glutathione-capped Quantum Dots for Plasma Membrane Labeling and Membrane Potential Imaging.* Nano Research, 2019. **12**: p. 1321-1326.
62. Zhao, Y., et al., *Wireless activation of neurons in brain slices using nanostructured semiconductor photoelectrodes.* Angew Chem Int Ed Engl, 2009. **48**(13): p. 2407-10.
63. *Qtracker non-targeted quantum dots for in vivo imaging*, in *Thermofisher*, ThermoFisher, Editor. 2007: Thermofisher.com.
64. Gil, H.M., et al., *NIR-quantum dots in biomedical imaging and their future.* iScience, 2021. **24**(3): p. 102189.
65. Wegner, D., Hildebrandt, N, *Quantum dots: Bright and Versitile in vitro and in vivo fluorescence imaging biosensors.* Royal Society of Chemistry, 2015. **44**.
66. Sonawane, G.H., Patil, S.P., Sonawane, S.H, *Nanocomposities and its Applications*. Applications of Nanomaterials, Esevier. 2018: Elsevier.
67. Li, C. and P. Wu, *Cu-doped quantum dots: a new class of near-infrared emitting fluorophores for bioanalysis and bioimaging.* Luminescence, 2019. **34**(8): p. 782-789.

68. Zhang, Y., et al., *Controlled Synthesis of Ag(2) Te@Ag(2) S Core-Shell Quantum Dots with Enhanced and Tunable Fluorescence in the Second Near-Infrared Window.* Small, 2020. **16**(14): p. e2001003.
69. Van Embden, J., Chesman, A., Jasieniak, J, *The Heat-Up Synthesis of Collodial Nanoparticles.* Chemistry of Materials, 2015. **27**: p. 2246-2285.
70. Wei, X., Al Muyeed, S.A., Peart, M.R., Sun, W., Tansu, N., Wierer Jr, J.J, *Room Temperature Luminescence of Passivated Ingan Quantum Dots formed by Quantum Sized Controlled Photoelectrochemical Etching.* Applied Physics, 2018. **113**: p. 121106.
71. Ballou, B., et al., *Noninvasive imaging of quantum dots in mice.* Bioconjug Chem, 2004. **15**(1): p. 79-86.
72. Daou, T.J., et al., *Effect of poly(ethylene glycol) length on the in vivo behavior of coated quantum dots.* Langmuir, 2009. **25**(5): p. 3040-4.
73. Al-Jamal, W.T., et al., *Lipid-quantum dot bilayer vesicles enhance tumor cell uptake and retention in vitro and in vivo.* ACS Nano, 2008. **2**(3): p. 408-18.
74. Petryayeva, E., W.R. Algar, and I.L. Medintz, *Quantum dots in bioanalysis: a review of applications across various platforms for fluorescence spectroscopy and imaging.* Appl Spectrosc, 2013. **67**(3): p. 215-52.
75. Huang, N., et al., *Efficacy of NGR peptide-modified PEGylated quantum dots for crossing the blood-brain barrier and targeted fluorescence imaging of glioma and tumor vasculature.* Nanomedicine, 2017. **13**(1): p. 83-93.
76. Shampa Ghosh, B.S., Punya Sachdeva, Vishal Chaudhary, Gokana Mohana Rani, Jitendra Kumar Sinha, *Graphene Quntum Dots as a Potential Diagnostic and Therapeutic Tool for the Management of Alzheimer's Disease.* Carbon Letters, 2022. **32**: p. 1381-1394.
77. Xiao, S., et al., *Graphene quantum dots conjugated neuroprotective peptide improve learning and memory capability.* Biomaterials, 2016. **106**: p. 98-110.
78. Chakraborty, P., et al., *Quantum dots: The cutting-edge nanotheranostics in brain cancer management.* J Control Release, 2022. **350**: p. 698-715.
79. Das, S. and P.A. Marsden, *Angiogenesis in glioblastoma.* N Engl J Med, 2013. **369**(16): p. 1561-3.
80. Kitambi, S.S., et al., *Retraction Notice to: Vulnerability of Glioblastoma Cells to Catastrophic Vacuolization and Death Induced by a Small Molecule.* Cell, 2017. **170**(2): p. 407.
81. Dorand, R.D., et al., *Comparison of intravital thinned skull and cranial window approaches to study CNS immunobiology in the mouse cortex.* Intravital, 2014. **3**(2).
82. Lathia, J.D., et al., *Direct in vivo evidence for tumor propagation by glioblastoma cancer stem cells.* PLoS One, 2011. **6**(9): p. e24807.
83. Osswald, M., et al., *Brain tumour cells interconnect to a functional and resistant network.* Nature, 2015. **528**(7580): p. 93-8.
84. Venkataramani, V., et al., *Glutamatergic synaptic input to glioma cells drives brain tumour progression.* Nature, 2019. **573**(7775): p. 532-538.
85. Venkataramani, V., et al., *Glioblastoma hijacks neuronal mechanisms for brain invasion.* Cell, 2022. **185**(16): p. 2899-2917 e31.
86. Schubert, M.C., et al., *Deep intravital brain tumor imaging enabled by tailored three-photon microscopy and analysis.* Nat Commun, 2024. **15**(1): p. 7383.
87. Wen, C.J., et al., *Theranostic liposomes loaded with quantum dots and apomorphine for brain targeting and bioimaging.* Int J Nanomedicine, 2012. **7**: p. 1599-611.
88. Jackson, H., et al., *Quantum dots are phagocytized by macrophages and colocalize with experimental gliomas.* Neurosurgery, 2007. **60**(3): p. 524-9; discussion 529-30.
89. Fan, H.Y., et al., *Graphene quantum dots (GQDs)-based nanomaterials for improving photodynamic therapy in cancer treatment.* Eur J Med Chem, 2019. **182**: p. 111620.
90. Nobari, S.A., Doustvandi, M.A., Yaghoubi, S.M., Oskouei, S.S., Alizadeh, E., Nour, M.A., Khiabani, N.A., Baradaran,B., Rahmati, M., *Emerging Trends in Quantum Dot Based Photosensitzers for Enhanced Photodynamic Therapy in Cancer Treatment.* Journal of Pharmaceutical Investigation, 2024.
91. Doustvandi, M.A., et al., *Photodynamic therapy using zinc phthalocyanine with low dose of diode laser combined with doxorubicin is a synergistic combination therapy for human SK-MEL-3 melanoma cells.* Photodiagnosis Photodyn Ther, 2019. **28**: p. 88-97.
92. Mansoori, B., et al., *Photodynamic therapy for cancer: Role of natural products.* Photodiagnosis Photodyn Ther, 2019. **26**: p. 395-404.
93. Donnelly, R.F., P.A. McCarron, and M.M. Tunney, *Antifungal photodynamic therapy.* Microbiol Res, 2008. **163**(1): p. 1-12.
94. Jiao, M., et al., *Aqueous Grown Quantum Dots with Robust Near-Infrared Fluorescence for Integrated Traumatic Brain Injury Diagnosis and Surgical Monitoring.* ACS Nano, 2024. **18**(29): p. 19038-19053.
95. Liu, Y., et al., *Synergistic Inhibitory Effect of GQDs-Tramiprosate Covalent Binding on Amyloid Aggregation.* ACS Chem Neurosci, 2018. **9**(4): p. 817-823.
96. Hu, Y., et al., *Application of quantum dots in brain diseases and their neurotoxic mechanism.* Nanoscale Adv, 2024. **6**(15): p. 3733-3746.

 doi:10.20944/preprints202411.0856.v1



97. Zhang, M.Z., et al., *Targeted quantum dots fluorescence probes functionalized with aptamer and peptide for transferrin receptor on tumor cells.* Nanotechnology, 2012. **23**(48): p. 485104.
98. Paris-Robidas, S., et al., *Internalization of targeted quantum dots by brain capillary endothelial cells in vivo.* J Cereb Blood Flow Metab, 2016. **36**(4): p. 731-42.
99. Zhao, M.X. and B.J. Zhu, *The Research and Applications of Quantum Dots as Nano-Carriers for Targeted Drug Delivery and Cancer Therapy.* Nanoscale Res Lett, 2016. **11**(1): p. 207.
100. McHugh, K.J., et al., *Biocompatible Semiconductor Quantum Dots as Cancer Imaging Agents.* Adv Mater, 2018. **30**(18): p. e1706356.